Cerebral Cortex September 2015;25:2970–2979
doi:10.1093/cercor/bhu094
Advance Access publication May 8, 2014

Transplantation of GABAergic Interneurons into the Neonatal Primary Visual Cortex Reduces Absence Seizures in Stargazer Mice

Mohamed Hammad[1], Stephen L. Schmidt[3,4,5,6], Xuying Zhang[1], Ryan Bray[1], Flavio Frohlich[3,4,5,6] and H. Troy Ghashghaei[1,2]

[1]Department of Molecular Biomedical Sciences, Center for Comparative Medicine and Translational Research, College of Veterinary Medicine, [2]Program in Genetics, North Carolina State University, Raleigh, NC 27607, USA, [3]UNC Department of Psychiatry, [4]Department of Cell Biology and Physiology, [5]Department of Biomedical Engineering and [6]Neuroscience Center, University of North Carolina at Chapel Hill, Chapel Hill, NC 27599, USA

Address correspondence to Troy Ghashghaei, 1060 William Moore Drive, Raleigh, NC 27607, USA. Email: troy_ghashghaei@ncsu.edu

Epilepsies are debilitating neurological disorders characterized by repeated episodes of pathological seizure activity. Absence epilepsy (AE) is a poorly understood type of seizure with an estimated 30% of affected patients failing to respond to antiepileptic drugs. Thus, novel therapies are needed for the treatment of AE. A promising cell-based therapeutic strategy is centered on transplantation of embryonic neural stem cells from the medial ganglionic eminence (MGE), which give rise to gamma-aminobutyric acidergic (GABAergic) interneurons during embryonic development. Here, we used the Stargazer (Stg) mouse model of AE to map affected loci using c-Fos immunohistochemistry, which revealed intense seizure-induce activity in visual and somatosensory cortices. We report that transplantation of MGE cells into the primary visual cortex (V1) of Stg mice significantly reduces AE episodes and lowers mortality. Electrophysiological analysis in acute cortical slices of visual cortex demonstrated that Stg V1 neurons exhibit more pronounced increases in activity in response to a potassium-mediated excitability challenge than wild-types (WT). The defective network activity in V1 was significantly altered following WT MGE transplantation, associating it with behavioral rescue of seizures in Stgs. Taken together, these findings present MGE grafting in the V1 as a possible clinical approach in the treatment of AE.

Keywords: absence seizure, MGE transplantation, network activity, Stargazer, visual cortex

Introduction

Epilepsies are characterized by abnormal electrical discharges that result in convulsive or absence seizures affecting more than 50 million people worldwide (de Boer et al. 2008). Absence epilepsy (AE) occurs often in children and can have disruptive effects on learning and normal childhood functions due to disturbance of consciousness and attention (Killory et al. 2011; Tenney and Glauser 2013). AE is characterized by spike-wave electroencephalographic discharges that are thought to be generated within distinct cortical and thalamic areas, although the pathophysiology of the disease remains uncertain (Blumenfeld 2005; Meeren et al. 2005). Nevertheless, it is clear that AE discharges rapidly spread through cortico-thalamocortical (CTC) loops leading to generalization of synchronized oscillations (van Luijtelaar and Sitnikova 2006).

CTC loops function through excitatory (glutamatergic) projections between the thalamus and cortex (Sherman and Guillery 2011). Under physiological conditions, neuronal firing in excitatory projections is tightly controlled by local inhibitory interneurons that produce and secrete the neurotransmitter gamma-aminobutyric acid (GABA) throughout the cortex, and in the reticular nucleus of the thalamus (Sherman and Guillery 2011). Abnormal synchronization of CTC networks in AE may be partially linked to reduced GABAergic neurotransmission (Crunelli et al. 2012). Current antiepileptic drugs primarily target glutamatergic or GABAergic receptors and can be effective in suppressing seizures (Beydoun and D'Souza 2012). However, prolonged drug treatment can have serious side effects, and a substantial number of patients remain pharmacoresistant (Seneviratne et al. 2012). Thus, development of alternative clinical treatment strategies for various forms of epilepsy is a high priority.

Grafting GABAergic neurons that functionally integrate into various neuronal networks have recently emerged as a potential alternative approach to reduce seizures in rodent models of tonic–clonic epilepsy through elevation of inhibitory tone (Baraban et al. 2009; Thompson 2009; Calcagnotto et al. 2010; Waldau 2010; Hunt et al. 2013). The cellular source of these grafts is the medial ganglionic eminence (MGE), an embryonic structure where most GABAergic interneurons in the cerebral cortices are born (Anderson et al. 1997). A sufficient increase in inhibitory postsynaptic currents has been demonstrated after functional integration of MGE grafts into the host primary visual cortex (V1) (Southwell et al. 2010). Moreover, MGE grafting successfully reduces frequency of seizures (Baraban et al. 2009), seizure-associated inflammation (Waldau 2010), and seizure susceptibility (Calcagnotto et al. 2010). Here, we provide the first report on using c-Fos mapping for identification of target loci for MGE grafting in an established mouse model of AE (Stargazer, Stg). We found, also for the first time, that the V1 exhibits highly elevated c-Fos activity during prolonged seizures in Stgs. These novel findings led us to graft isolated wild-type (WT) MGE cells into the neonatal V1 in Stg mice resulting in robust rescue of AE phenotypes. Remarkably, the majority of MGE-grafted Stgs survived up to 4 months, whereas nearly all nontransplanted Stgs die shortly after weaning. Finally, we demonstrate with an in vitro electrophysiological assay that MGE transplanted cells reduced local excitability in V1 in response to a potassium excitability challenge.

Materials and Methods

Animals

Animal use was approved by the Institutional Animal Care and Use Committee at the North Carolina College of Veterinary Medicine. Heterozygous Stg mutants (*B6C3Fe a/a-Cacng2stg*), green fluorescent protein (GFP) transgenic mice (*C57BL/6-Tg(CAG-EGFP)1Osb/J*), and WT (*C57BL/6J*) mice were obtained from the Jackson Laboratory. MGE

grafts were extracted from embryonic day 12.5 (E12.5) GFP mice obtained from timed pregnant females. All animals were housed on 12-h light–dark cycle and given ad libitum access to food and water.

Analysis of Absence Seizures

Incidence of seizures in Stg mice was recorded and quantified daily during the light phase from postnatal day 14 (P14) to P21. For each observation, mice were transferred from their home cage to novel clean cages each equipped with 2 top-mounted CCTV cameras (SVAT VU5, Cheektowaga, NY, USA) positioned on the opposite walls of the cage affording a two-sided view. Mice were video recorded for 10 min. For c-Fos mapping, Stgs exhibiting a prolonged seizure (>20 s) were immediately moved back to their home cage and perfused 90 min later. For all other analyses, video recordings were analyzed and seizures were scored by recording the number and duration of freezing and head-tilting episodes. Data were normalized to reflect quantified parameters per hour.

Tissue Dissection and MGE Transplantations

Ventricular and subventricular domains of the MGE were microdissected from 250 µm coronal forebrain slices obtained from E12.5 GFP transgenic embryos as described previously (Jacquet et al. 2010). Injectates were prepared from cell suspensions of MGE dissected tissue as described by another group (Southwell et al. 2010) and collected in artificial cerebrospinal fluid (aCSF, 29 mM NaCl, 0.6 mM KCl, 0.2 mM $CaCl_2$, 0.3 mM $MgCl_2$, 0.1 M PBS, pH 7.4) supplemented with 10 ng of epidermal and fibroblast growth factors, and DNase I (50 µg/mL). P0 host mice were anesthetized by hypothermia, and the occipital cortices were bilaterally injected with 10^5 cells in each hemisphere (total volume 0.5 µL per injection), while the mice were stabilized on ice (G-Stg-V1 mice). Stereotactic coordinates were according to the Atlas of the Developing Mouse Brain (Paxinos et al. 2007): The injections in V1 were 0.1–0.3 mm rostral to lambda, and 1.7–2.2 mm lateral to midline. The depth of needle penetration was at 0.7 mm below the surface of the skull based on pilot studies. Control mice received bilateral injections of aCSF without cells (GStg-V1-aCSF), or were injected with dead MGE cells obtained from repeated frost and thaw at 100 °C (GStg-V1-DS). The initial number of MGE cells for dead cell control experiments were the same as live MGE experiments. Another set of controls received MGE grafts into their frontal cortices (coordinates: 3.4–3.8 mm rostral to lambda; 0.5–1.0 mm lateral to midline; 0.7 mm deep). All injections were performed at a rate of 100 nL per minute over a maximum of 5 min. Following surgery, mice were placed under a heating lamp until actively breathing and were returned to the dam until weaning. Ten transplanted MGE-grafted Stg mice were maintained until 4 months of age to determine a post-transplantation survival curve.

Perfusion and Tissue Processing

Experimental and control mice were overdosed with 2,2,2-tribromoethanol (Avertin, 400 mg/kg IP; Sigma), perfused intracardially with 4% formaldehyde in PBS, and their brains were removed and postfixed overnight (4 °C). Brain sections of 50 µm thickness were obtained sagittally (for stereological counts of GFP+ transplanted cells in V1) and coronally (for all other analyses) using a vibratome (Leica). Floating sections were immunostained with various markers using standard protocols. The following primary antibodies were used: mixture of rabbit anti-GABA (1 : 500; Millipore) and rabbit anti-GAD65/67 (1 : 1000; Sigma), chicken anti-GFP (1 : 1000; Abcam), mouse anti-NeuN (1 : 1000; Millipore), rabbit anti-Olig2 (1 : 1000; Millipore), rabbit anti-parvalbumin (PV; 1 : 1000; Millipore), mouse anti-GFAP (1 : 1000; Millipore), and goat anti-cFos (1 : 1000; Santa Cruz). The following secondary antibodies were used: cyanine 3 (Cy3)-conjugated donkey anti-mouse (1 : 1000; Millipore), goat anti-chicken Alexa 488-conjugated, donkey anti-rabbit Alexa 647-conjugated, and goat anti-mouse Alexa 647-conjugated (1 : 1000; Invitrogen). Sections were mounted and coverslipped using standard methods and imaged using a Nikon C1 confocal microscope.

Generation of histochemical libraries of c-Fos immunostained tissues was similar to methods described previously (Ghashghaei and Barbas 2002). Briefly, sections were processed for c-Fos immunohistochemistry 90 min after a prolonged seizure in Stgs (20 s or longer) or 10 min testing periods for WT mice after placing them in a novel clean cage without food or water. Brains were processed as above, and blocked and incubated with c-Fos antibody overnight. A biotinylated rabbit anti-goat secondary antibody and the ABC kit (Vector Laboratories) were used for peroxidase reaction with diaminobenzidine according to manufacturer's instructions. Sections were mounted and coverslipped using standard methods, and imaged using a Zeiss AxioImager M-1 microscope.

Quantification of Cellular Densities and Percentages

Densities of c-Fos+ nuclei in all cortical regions of WT and Stg mice were quantified using systematic optical density measurements by NIH ImageJ, following a similar approach to a previously published protocol (Ghashghaei and Barbas 2001). Optical measurements were normalized by subtraction of background intensities and averaged across data obtained from 3 mice within each genotype. To quantitatively characterize the neuronal and glial fate of GFP+ cells in V1 of MGE-grafted Stgs, sections were immunohistochemically labeled for NeuN (mature neurons), a mixture of GABA and GAD antibodies (GABAergic interneurons), PV (subset of GABAergic interneurons), Olig2 (oligodendrocytes), and GFAP (astrocytes). Percentages of transplanted GFP + cells colabeled with each marker were obtained from counting at least 60 GFP+ cells from a minimum of 3 sections through V1 in each of 10 GStg-V1 mice. Percentages of GABA+ and PV+ grafted neurons in various cortices were calculated by counting marker+ and DAPI+ nuclei in the same number of sections and animals as described above. Quantitated data were expressed as mean ± standard error of the mean (SEM), and significance was defined as $P < 0.05$ using Student's t-test. To assess if dosage of PV+ grafted cells correlated with degree of rescue in head tilts per hour, body weight, seizure duration, and minutes seizing per hour, a PV prevalence index (PVPI) was calculated as [%PV+ neurons] multiplied by [estimated density of GFP+ grafted cells] in V1 of each animal. PVPI and behavioral measures for each GStg-V1 mouse were then normalized to fall in a range of 0–100 (see chart in Fig. 4*C* later). The indices were then ranked and correlated with each normalized behavioral index using Pearson's correlation.

Densities of GFP+ cells in V1 were determined using standard stereological cell counting protocols described before (Ghashghaei and Barbas 2002; Ghashghaei et al. 2007). Briefly, brains were cut in the sagittal plane, and Z-stack tiles of confocal images from a single series of brain sections labeled for GFP and DAPI were obtained in V1 using an oil immersion 60× lens on a Nikon C-1 confocal microscope (z-intervals of 1 µm). Confocal z-stacks were obtained excluding 2 µm of the top and bottom surfaces of sections (guard zones) to avoid potential false-negative and -positive counts due to cell plucking and staining artifacts. Counting and estimation of cell numbers were conducted using the StereoInvestigator software (UNC Neuroscience Center, Imaging Core Facility). About 200-µm sampling grids were set such that 3–10 sampling sites were obtained for V1 within each section. Counts were obtained in 50 × 50 µm counting frames (dissectors) with standard stereological inclusion and exclusion borders (West and Gundersen 1990). Estimates of cell numbers and V1 volume were transferred to Microsoft Excel for the calculation of densities.

Pilot studies were conducted for each animal, and once stereological parameters were established they were kept identical for subsequent V1 measurements despite changes in the size of V1 across sections. A variability threshold was established such that more sections were used for counting until within-animal sampling errors (SEM) were ≤10% of estimated cell numbers in sampled areas within V1. Counts were obtained from a minimum of 5–8 sections that included V1 per animal. Data were obtained in a minimum of 3 independent animals from each experimental group.

Electrophysiological Recordings and Analyses

Acute neocortical slices were prepared from juvenile control Stg mice (ungrafted Stg, GStg-V1-dead cell, or GStg-V1-aCSF mice; all P14–P21), MGE-grafted Stgs (GStg-V1), and WT mice after deep anesthesia with Euthasol. Brains were collected in ice-cold sucrose solution and sliced

coronally at 200 µm using a vibratome (VT1000S, Leica). Slices including V1 were allowed to recover while incubating in aCSF bubbled with carbogen for 45 min at 34 °C. Neurophysiological recordings were conducted using perforated arrays of 60 electrodes (30 µm diameter) and 200 × 200 µm spacing in a MEA 2100 (Multichannel Systems, Reutlingen, Germany). Slices were initially perfused with control aCSF (1800 s control epoch) followed by perfusion with aCSF containing 5 mM of KCl (elevated K^+ aCSF) for 1800 s. Cortical layers were mapped to individual recording electrodes by measuring the relative position of the electrode between pia and white matter. Raw traces were recorded from 60 electrodes simultaneously using MC_Rack (Multichannel Systems), sampled at 25 kHz. Raw data were high-pass filtered with a 300-Hz and the noise level calculated by the standard deviation of the recorded signal on each electrode. Action potentials (APs) were identified by crossing −4 times the noise level of that electrode.

MEA data from electrodes in V1 were analyzed with custom-written scripts in Matlab (Mathworks, Natick, MA, USA) as detailed previously (Schmidt et al. 2013). Briefly, activity time courses for each slice were determined by calculating mean spikes per electrode in 20 s bins across all stable electrodes in V1. The last 300 s of the each 1800-s interval were used for all subsequent analyses. The effect size of K^+ was calculated as the firing rate (FR) of each electrode in aCSF with elevated K^+ divided by the FR of the electrode in control aCSF. The spectra of 1 ms binned whole-slice spike trains were calculated using convolution for wavelets between the 1 and 40 Hz. The change in oscillatory structure was calculated by dividing the spectrum of each slice in elevated K^+ aCSF by the spectrum calculated from control aCSF data. To analyze nonoscillatory network synchrony, we examined correlations of pair spike trains with 100 ms bins. Electrode pairs with correlation <0.1 for both intervals were excluded from analysis. Statistical significance was determined using Kruskal–Wallis tests in conjunction with Tukey's multiple comparison tests at $P < 0.05$. These tests compute confidence intervals at $P = 0.05$, if the confidence intervals of two groups do not overlap, then $P < 0.05$.

Results

Quantification of Stg Phenotypes

Mice homozygous for the Stg mutation (Letts et al. 1998) develop neurological symptoms characterized by severe ataxia, abnormal motor behavior, cervical dystonia, and high frequency of absence-like seizures during the second and third postnatal weeks. Using the stereotypical upward head tilt and motor freezing as behavioral readouts, we recorded an average of 86 ± 7 seizures per hour with average durations of 24 ± 2 s for each episode ($n = 10$ mice from 4 independent litters at P14–P21). Stgs also failed to gain weight at the same rate as their WT or heterozygous littermates. This difference was most pronounced at P21, when Stgs weighed 4.9 ± 1.4 g less than their WT siblings ($n = 20$ mice from 11 litters). Stg mice perished on average 29 (±3) days postnatal.

c-Fos Mapping of the Stg Forebrain Reveals Elevated Activity in Visual and Somatosensory Cortices

To identify target loci for an MGE transplantation approach in Stg brains, we mapped c-Fos immunoreactivity, which is an established biomarker for neuronal activity. To eliminate possible differential behavioral states of mice in their home cages at the time of testing, mice were placed in a novel clean

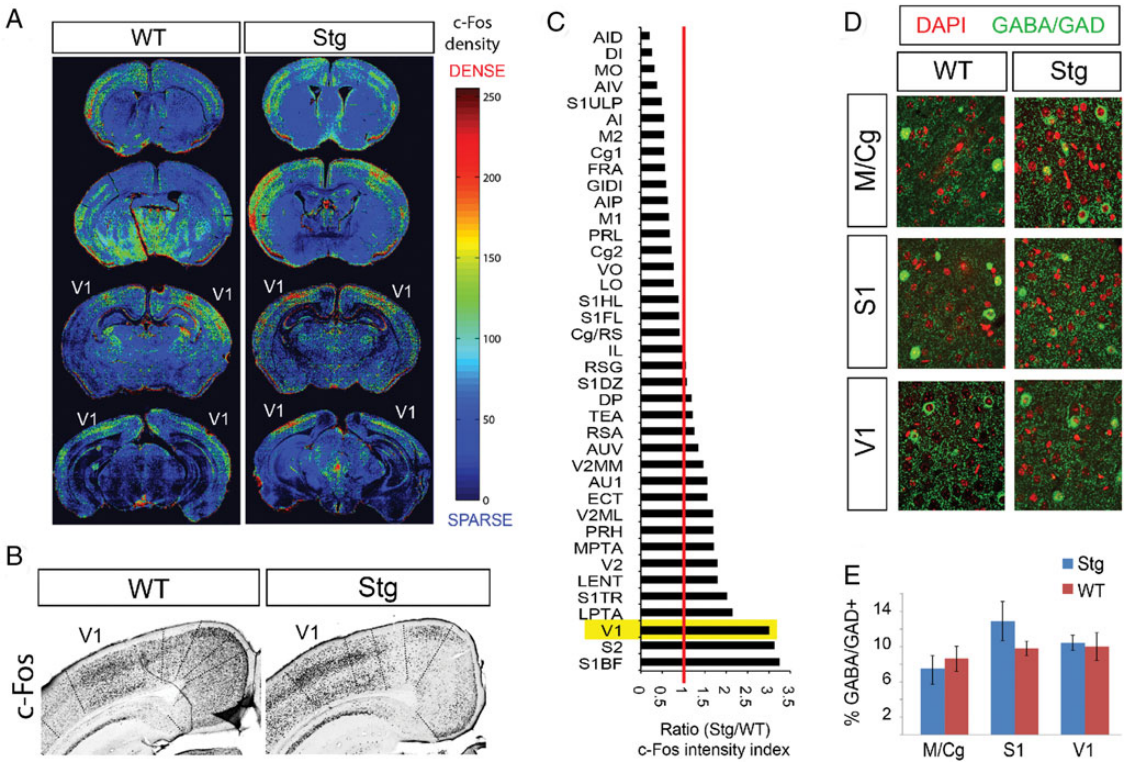

Figure 1. Mapping and quantification of c-Fos expression following prolonged absence seizures (AE) in Stg mice. (*A*) Representative confocal heat maps of c-Fos immunoreactivity in WT and Stg brains at 4 rostrocaudal levels (relative to bregma; top: +0.14 mm, −0.82 mm, −2.3 mm, and −3.28 mm: bottom). (*B*) Representative images of immunohistochemically stained cortices containing c-Fos+ nuclei (black) in V1 of WT and Stg brains. (*C*) Ratios of pixel densities of c-Fos immunoreactivity in cortical areas (*y*-axis) of Stgs compared with WT brains. Cortical areas are labeled according to a mouse brain atlas (Paxinos and Franklin 2001). Ratios were calculated from normalized density measures of c-Fos+ nuclei within each area ($n = 3$ mice per group). See Table 1 for more details and abbreviations. (*D*) Representative confocal micrographs of GABA/GAD+ neurons and processes (green) in tissues (M/Cg, S1, and V1) counterstained with a nuclear marker (DAPI, red). (*E*) Percentages of GABA/GAD+ cells calculated over all DAPI+ nuclei in the 3 identified cortical areas.

environment without food or water and Stgs were monitored for the occurrence of a prolonged seizure (>20 s). Mice were sacrificed 90 min later followed by tissue processing for c-Fos labeling (Fig. 1*A*). Optical density measurements of c-Fos immunoreactivity revealed significant differences between cerebrocortical areas in WTs and Stgs. WT forebrains were characterized by strong c-Fos expression in dorsomedial cortices, including the motor and cingulate areas (M1, M2, Cg1, Cg2, referred to M/Cg hereafter; Fig. 1*B* and Table 1). In contrast, intense labeling was seen in primary somatosensory (S1) and visual (V1) cortical areas of Stg mice compared with WTs (Fig. 1*B*,*C* and Table 1). To evaluate if the disruption of c-Fos expression levels was correlated with a potential change in the number of GABAergic interneurons in affected cortices, we assessed the proportion of GABA/GAD+ interneurons over all cells in V1, S1, and M/Cg cortices. There were no significant differences in the percentages of GABA/GAD+ neurons (over all DAPI+ nuclei) in any of the selected cortices (Fig. 1*D*,*E*), suggesting that the proportion of GABAergic interneurons does not appear to correlate with the Stg seizure phenotypes. However, since activation of GABAergic neurons in the Stg cortex was recently shown to be faulty (Maheshwari et al. 2013), we reasoned that elevated c-Fos activity in V1 and S1 may be due to defective GABAergic neurons in the Stg cortex. Thus, we asked if grafting WT MGE cells into V1 improves the aberrant network activity associated with AE seizures in Stg mice.

MGE Grafting in V1 Significantly Reduces AE Seizures and Postnatal Mortality in Stg Mice

Initial attempts to graft MGE cells into juvenile (P14–P21) Stg brains largely failed due to the fragile health of these mice, which resulted in high mortality either during anesthesia or shortly after surgery. This prompted us to target our transplantations to the cortex of new-born animals (Fig. 2*A*). MGE cells were harvested from forebrains of embryonic day 12.5 (E12.5) transgenic mice ubiquitously expressing the GFP and delivered focally into V1 of neonatal Stg mice (GStg-V1; Fig. 2*A*). Low densities of GFP+ cells were observed in V1 3–4 weeks after

Table 1

Average optical density measures of c-Fos immunoreactivity in cortical areas of Stg, WT, and GStg-V1 mice when placed in a novel environment

	Stg	WT	GStg-V1	Stg/WT (sig.)	GStg-V1/WT (sig.)
AID	17.62 ± 1.9	90.61 ± 12.0	108.22 ± 18.7	0.19 (***)	1.19 (NS)
DI	20.58 ± 1.3	83.29 ± 8.1	89.45 ± 8.7	0.25 (***)	1.07 (NS)
MO	24.76 ± 1.8	80.15 ± 11.2	96.44 ± 12.3	0.31 (***)	1.20 (NS)
AIV	28.72 ± 4.2	79.17 ± 9.5	64.21 ± 9.2	0.36 (***)	0.81 (NS)
S1J/ULP	30.99 ± 5.2	65.49 ± 6.7	49.64 ± 5.2	0.47 (***)	0.76 (**)
AI	39.94 ± 5.4	76.03 ± 9.3	88.64 ± 10.3	0.53 (***)	1.17 (NS)
M2	33.42 ± 5.9	63.22 ± 5.8	69.45 ± 7.3	0.53 (***)	1.10 (NS)
Cg1	40.44 ± 2.1	76.4 ± 7.9	70.14 ± 9.3	0.53 (***)	0.92 (NS)
FRA	38.82 ± 5.1	70.94 ± 8.4	53.21 ± 6.8	0.55 (***)	0.75 (*)
GIDI	43.57 ± 3.8	76 ± 10.1	83.66 ± 9.3	0.57 (***)	1.10 (NS)
AIP1	34.43 ± 4.3	55.98 ± 4.9	60.21 ± 5.7	0.62 (***)	1.08 (NS)
M1	37.61 ± 3.6	58.12 ± 3.7	50.2 ± 9.3	0.65 (***)	0.86 (NS)
PRL	47.51 ± 2.2	72.26 ± 9.0	113.57 ± 16.8	0.66 (***)	1.57 (***)
Cg2	49.24 ± 5.9	70.31 ± 4.7	56.33 ± 11.3	0.70 (**)	0.80 (NS)
VO	54.43 ± 5.6	72.57 ± 3.9	73.23 ± 6.2	0.75 (*)	1.01 (NS)
LO	55.25 ± 7.5	73.23 ± 6.1	88.32 ± 12.2	0.75 (*)	1.21 (NS)
S1HL	45.16 ± 7.1	51.79 ± 3.8	56.75 ± 4.2	0.87 (NS)	1.10 (NS)
S1FL	45.57 ± 3.8	51.93 ± 4.6	69.33 ± 7.1	0.88 (NS)	1.34 (**)
Cg/RS	57.26 ± 8.2	64.49 ± 3.3	76.32 ± 11.8	0.89 (NS)	1.18 (NS)
IL	57.76 ± 2.8	60.82 ± 6.3	42.34 ± 9.5	0.95 (NS)	0.70 (**)
RSG	69.71 ± 4.5	66.82 ± 2.2	65.87 ± 10.9	1.04 (NS)	0.99 (NS)
S1DZ	46.99 ± 3.1	44.31 ± 6.7	59.67 ± 5.1	1.06 (NS)	1.35 (*)
DP	43.04 ± 5.3	36.71 ± 4.8	37.55 ± 4.8	1.17 (NS)	1.02 (NS)
TEA	71.33 ± 8.1	59.58 ± 10.0	75.86 ± 3.3	1.20 (NS)	1.27 (*)
RSA	83.73 ± 14.3	67.61 ± 13.1	78.65 ± 7.7	1.24 (NS)	1.16 (NS)
AUV	81.05 ± 6.7	60.99 ± 5.2	66.21 ± 6.3	1.33 (**)	1.09 (NS)
V2MM	86.26 ± 4.8	59.62 ± 3.1	90.22 ± 12.9	1.45 (***)	1.51 (***)
AU1	85.19 ± 17.3	55.28 ± 12.5	48.49 ± 8.6	1.54 (NS)	0.88 (NS)
ECT	74.05 ± 4.6	47.84 ± 2.2	38.92 ± 4.2	1.55 (***)	0.81 (NS)
V2ML	97.1 ± 9.3	58.01 ± 3.3	89.44 ± 12.2	1.67 (***)	1.54 (*)
PRH	80.09 ± 8.3	47.52 ± 6.1	70.29 ± 6.8	1.69 (***)	1.48 (**)
MPTA	58.32 ± 7.5	34.46 ± 6.4	40.11 ± 9.2	1.69 (*)	1.16 (NS)
V2	91.05 ± 3.3	51.21 ± 4.0	63.22 ± 7.6	1.78 (***)	1.23 (NS)
LENT	79.04 ± 9.8	44.34 ± 2.7	38.51 ± 5.8	1.78 (***)	0.87 (NS)
S1TR	64.6 ± 6.7	32.28 ± 5.2	41.38 ± 6.3	2.00 (***)	1.28 (NS)
LPTA	62.3 ± 8.7	29.18 ± 3.9	22.83 ± 7.2	2.14 (***)	0.78 (NS)
V1	96.15 ± 8.3	33.65 ± 2.2	49.55 ± 3.3	2.86 (***)	1.47 (**)
S2	74.45 ± 5.3	23.92 ± 1.1	35.82 ± 7.8	3.11 (***)	1.50 (*)
S1BF	76.8 ± 4.1	23.77 ± 2.8	32.24 ± 4.6	3.23 (***)	1.36 (*)

Abbreviations matching those in the mouse brain map of Paxinos and Franklin: AID, agranular insular cortex, dorsal; DI, dysgranular insular cortex; MO, medial orbital cortex; AIV, agranular insular cortex, ventral; S1/ULP, primary somatosensory cortex, upper lip region; AI, agranular insular cortex; M2, secondary motor cortex; Cg1, cingular cortex, area 1; FRA, frontal association cortex; GIDI, granular and dysgranular insular cortex; AIP, agranular insular cortex; M1, primary motor cortex; PRL, prelimbic cortex; Cg2; cingular cortex, area 2; VO, ventral orbital cortex; LO, lateral olfactory tract; S1HL, primary somatosensory cortex, hindlimb region; S1FL, primary somatosensory cortex, forelimb region; Cg/RS, cingular/retrosplenial cortex; IL, infralimbic cortex; RSG, retrosplenial granular cortex; S1DZ, primary somatosensory cortex, dysgranular region; DP, dorsal peduncular cortex; TEA, temporal association cortex; RSA, retrosplenial agranular cortex; AUV, secondary auditory cortex, ventral area; V2MM, secondary visual cortex, mediomedial area; AU1, primary auditory cortex; ECT, ectorhinal cortex; V2ML, secondary visual cortex, mediolateral area; PRH, perirhinal cortex; MPTA, medial parietal association cortex; V2, secondary visual cortex; LENT, lateral entorhinal cortex; S1TR, primary somatosensory cortex, trunk region; LPTA, lateral parietal association cortex; V1, primary visual cortex; S2, secondary somatosensory cortex; S1BF, primary somatosensory cortex, barrel field.

Normalized optical density data are listed as mean ± SEM ($n = 3$ animals/area). Significance was determined by Student's *t*-test: $^{*}P < 0.05$; $^{**}P < 0.01$; $^{***}P < 0.001$; NS, not significantly different.

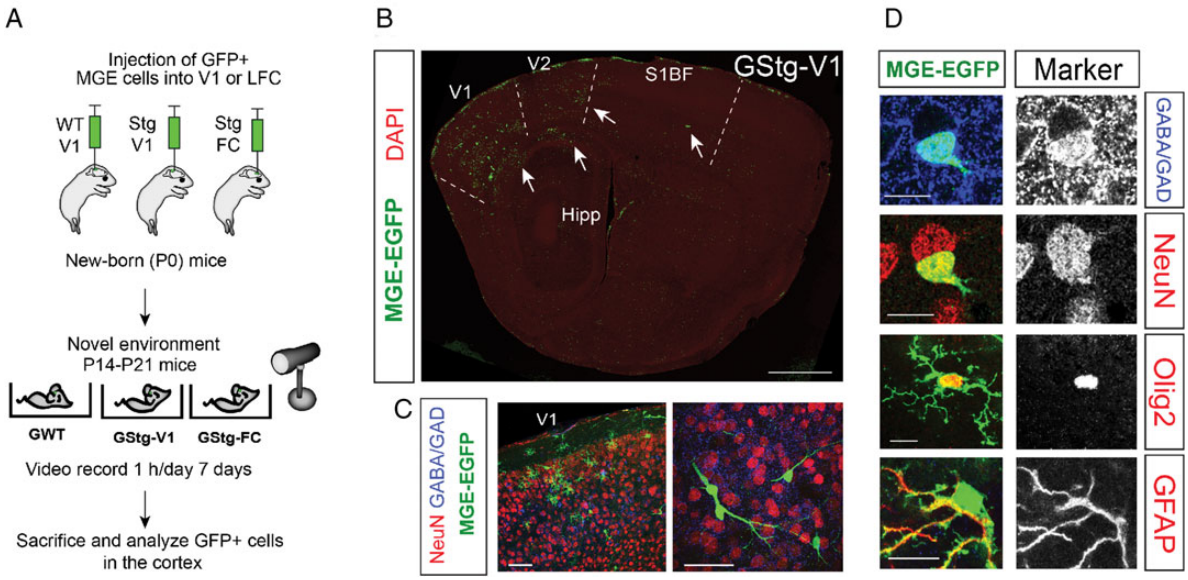

Figure 2. MGE cells transplanted in V1 differentiate into GABAergic interneurons. (*A*) Schema of bilateral WT MGE transplantation into V1 or frontal cortices (FC) of P0 Stg recipients. (*B*) Low power image of MGE-GFP transplanted V1 in a P21 brain with minimal degree of cell spreading (arrows) into adjacent V2, S1BF, or hippocampus (Hipp) tissues. Tissue was counterstained with DAPI (blue) for cytoarchitectonic mapping. Scale bars = 1 mm. (*C*) Higher power images of GFP+ MGE-derived cells found in V1 at the age of P21 (co-stained with NeuN, red; and GABA/GAD, blue). Scale bars = 50 μm. (*D*) The majority of the MGE cells in V1 3 weeks post-transplantation had differentiated into GABAergic (GABA/GAD, blue) neurons (NeuN, red; same GFP+ neuron). Smaller fractions were oligodendrocytes (Olig2+) and astrocytes (GFAP+). Scale bars = 10 μm.

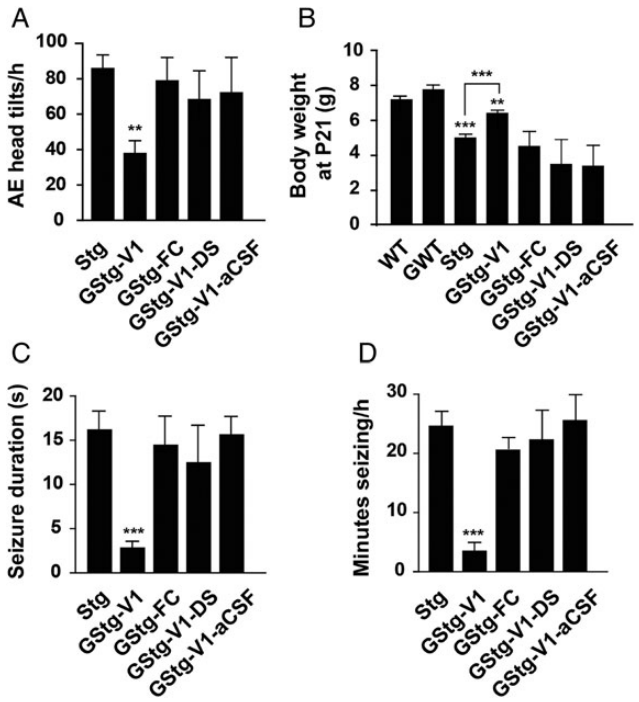

Figure 3. Transplantation of MGE cells in V1 of Stgs alleviates AE seizures. The following behavioral measurements showed a significant change in MGE-grafted Stgs (GStg-V1) compared with frontal cortex-grafted (GStg-FC), non-grafted, V1 dead cell-grafted (GStg-V1-DS), or V1 saline injected (GStg-V1-aCSF) control Stg mice at the age of P21: (*A*) average head tilts per hour; (*B*) body weight (g); (*C*) average duration of individual seizures (s); (*D*) average minutes per hour spent in seizures. Data are mean ± SEM. Significance was determined by Student's *t*-test; $^{**}P < 0.05$, $^{***}P < 0.01$. MGE, medial ganglionic eminence; WT, wildtype; GWT, MGE-grafted wildtype.

grafting (Fig. 2*B*,*C*). Stereological density estimation of GFP+ cells in GStg-V1 demonstrated a low yield of integration (2340 ± 290 cells/mm^3 of V1; $n = 10$ mice). The few integrated cells had differentiated into 73 ± 3% neurons (NeuN+); of which, 93 ± 4% were GABAergic (GABA/GAD+). Moreover, 14 ± 6% of all GFP+ cells in V1 were oligodendrocytes (Olig2+) and 3 ± 1% astrocytes (GFAP+; $n = 3$ mice, 60 cells per animal and per marker). A few GFP+ cells were also found in the hippocampus, amygdala, subthalamic nuclei, basal forebrain territories, and white matter (and sporadically in other regions), but the majority were situated in V1 and nearby cortices (88 ± 3% of total cells counted per animal; 60 cells/animal; $n = 10$ mice). Taken together, these analyses indicate that MGE-derived neuronal and glial lineages integrated and differentiated in V1 after grafting, albeit at low densities (Fig. 2*D*).

Effects of MGE transplantations became immediately apparent as GStg-V1 mice exhibited a significant decrease in AE episodes (measured by reduced frequency of stereotypic head tilt episodes) compared with control sham-grafted Stg mice (Fig. 3*A*; 53 ± 0.15% reduction, $n = 10$ mice per group, $P < 0.05$). Moreover, GStg-V1 mice gained more weight than their control littermates by P21 (Fig. 3*B*), and 8 of 10 GStg-V1 mice survived up to 4 months compared with none in the ungrafted group. Concomitantly, the duration of individual AE events was significantly decreased in GStg-V1 mice (89 ± 0.02% reduction, $P < 0.05$, $n = 10$ per genotype and condition; Fig. 3*C*) and average time spent in seizures declined by 81 ± 0.9% ($n = 10$, $P < 0.05$; Fig. 3*D*). Phenotypes unrelated to the CTC loop (e.g., ataxia) were unaffected in GStg-V1 mice. Importantly, neither sham injections into V1 (dead cells, GStg-V1-DS; or vehicle, GStg-V1-aCSF), nor MGE grafting in the frontal cortices (GStg-FC), attenuate seizure frequency or duration (Fig. 3). Thus, surgical manipulation alone or off-target transplantation failed to repeat the effects of MGE grafting in V1 on AE seizures.

MGE Grafting Alters Cortical Network Activity in GStg-V1 Brains

To determine if altered AE seizures and survival in GStg-V1 mice were correlated with changes in global cortical activity,

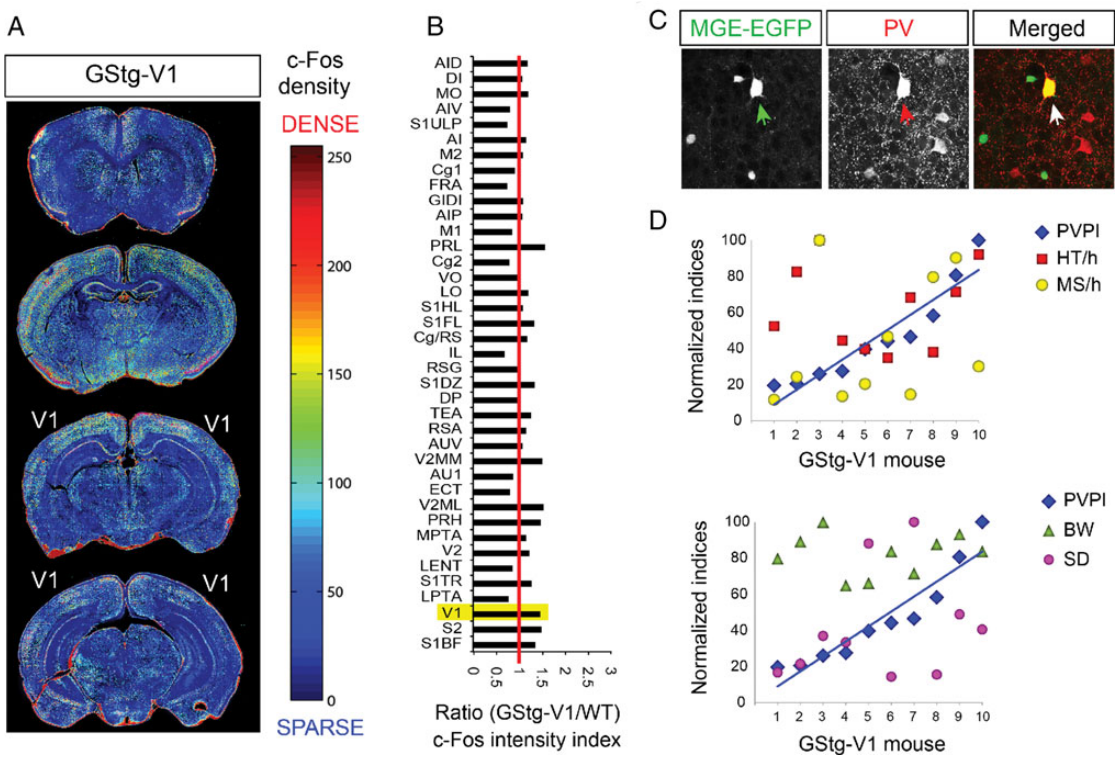

Figure 4. Analysis of c-Fos expression and PV prevelance in the GStg cortex. (*A*) Representative confocal heat maps of c-Fos immunoreactivity in G-Stg-V1 brains at 4 rostrocaudal levels similar to those in Figure 1. (*B*) Ratios of pixel densities of c-Fos immunoreactivity in cortical areas (*y*-axis) of GStg-V1 mice compared with WT brains. Labeling and quantifications were conducted similar to what is described in Figure 1. See Table 1 for more details and abbreviations. (*C*) Example of a PV+ GFP+ transplanted neuron (arrows) in V1 of a GStg-V1 mouse. (*D*) Scatter plots of normalized PV prevalence indices (PVPI) and rescued indices normalized for each of 10 GStg-V1 mice (*x*-axis) measured 3–4 weeks post-transplantation. Normalized behavioral indices: HT/h, head tilts per hour; MS/h, minutes seizure per hour; BW, body weight; SD, seizure duration. PVPI data were ordered from lowest to highest in both plots (blue progression line). There is no correlation between PVPI and any of the rescued indices in GStg-V1 mice.

we conducted c-Fos mapping and optical densitometry in GStg-V1 cortices and compared them with Stg data from the first part of the study (Fig. 4*A*,*B*). Matching the behavioral changes, distribution of cortical c-Fos activity in M/Cg, S1, and V1 of GStg-V1 brains had shifted toward WT patterns (compare Fig. 1*A*,*C* with Fig. 4*A*,*B*). Thus, disappearance of stereotypic head tilting appeared highly correlated with changes in patterns of c-Fos activity throughout various cortices, implicating altered cortical activity in response to MGE transplantation in V1 as the mechanism for alleviation of AE seizures in GStg-V1 mice.

Since the excitability of PV expressing (PV+) fraction of GABAergic interneurons was recently shown to be selectively defective in the Stg cortex (Maheshwari et al. 2013), we assessed if the dosage of differentiating PV+ neurons correlated with degree of rescue measurement in the first part of the study (Fig. 4*C*). Only a small fraction of grated cells were PV+ in V1 of GStg mice (13 ± 2%; $n = 10$; Fig. 4*C*). Nevertheless, values obtained from Pearson's correlation applied to comparison of incidence of PV+ grafted cells in V1 in individual GStg-V1 animals failed to show any correlation with their degree of head-tilting ($r = 0.20$), body weight ($r = 0.17$), seizure duration ($r = 0.15$), or seizure incidence ($r = 0.27$) (Fig. 4*C*). This analysis indicates that the few integrated GABAergic neurons in V1 were sufficient in changing patterns of c-Fos activity in the Stg brain without an obvious correlation with their PV identity.

To further establish the neurophysiological correlates of the pronounced effects of MGE grafting on behavioral and cortical c-Fos activities in GStg-V1 mice, we studied network excitability in acute cortical slices containing V1 using multielectrode array recordings. Activity was simultaneously recorded from an average of 28 electrodes in V1 per slice (Fig. 5*A*), and spontaneous APs were extracted from each channel (Fig. 5*B*). We hypothesized that MGE-derived neurons reduce network activity in V1 under conditions of heightened excitability in comparison to the untreated Stg V1. To test this hypothesis, baseline activity levels in control aCSF were established and compared with activity in elevated K^+ aCSF (Fig. 5*C*).

Slices from WT, control (ungrafted Stg, GStg-V1-dead cell, or GStg-V1-aCSF), and GStg-V1 animals all exhibited increased network activity in elevated K^+; however, this increase was more pronounced and the time course was steeper in cortical slices from Stgs. In contrast, GStg-V1 slices displayed an intermediate response between WT and Stg (Fig. 5*D*; $n = 14$ WT slices, black; 17 control Stg slices [6 Stg, 6 GStg-V1-dead cell, and 5 GStg-V1-aCSF], red; 18 GStg-V1 slices). To quantify the change in excitability, we computed the effect size of K^+ administration by dividing the elevated K^+ FR by the control FR (Fig. 6*A*). In agreement with the averaged time course data, the effect size of elevated K+ for control Stg slices was significantly greater than values for both WT and GStg-V1 slices, and importantly, WT and GStg-V1 effect sizes were not significantly different (0.49 ± 0.03 for WT, 0.79 ± 0.03 for Stg, and 0.52 ± 0.03 for GStg-V1; all values are $\log_{10}$; $n = 376$, 432, and 583 electrodes, respectively, significant at $P < 0.05$). These data indicate that MGE grafting reduced the increase in spontaneous activity in response to an excitability challenge toward

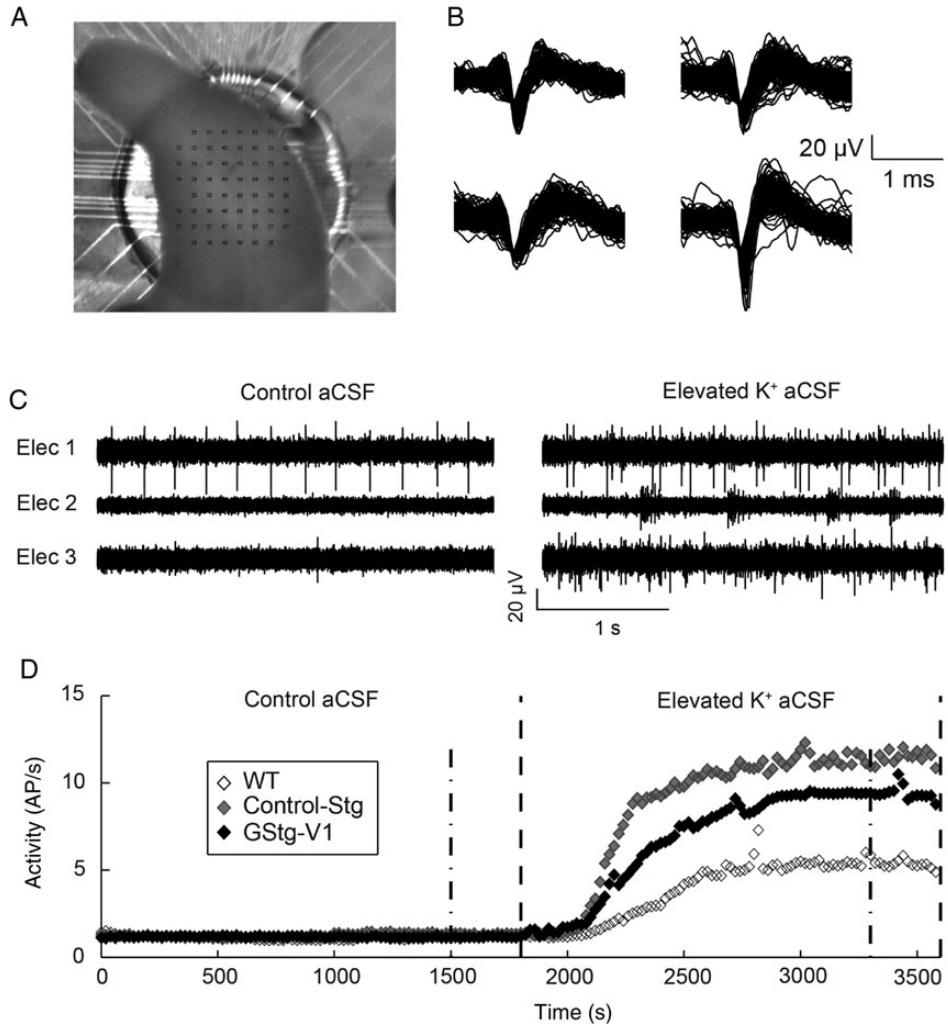

Figure 5. MGE grafting reduced network excitability measured in acute cortical slices. (*A*) A slice on the multielectrode array with electrodes superimposed as dots. (*B*) Example APs from 4 different electrodes (150 APs per electrode are displayed). (*C*) Example multiunit traces from 3 electrodes for a slice in control aCSF. Recordings from the same electrodes after elevated K^+ aCSF exposure exhibit increased excitability. (*D*) Median whole-slice time courses of spontaneous activity for WT (open diamonds), Stg (gray diamonds), and GStg-V1 (black diamonds). Dashed/dotted lines delineate intervals for which average firing rates were computed. Slices of all groups increased activity when elevated K^+ aCSF was applied. Stg slices exhibited the largest increase in excitability, whereas WT slices exhibit the smallest change in excitability.

levels measured in WT slices. This reduction in modulation of firing rate by elevated K^+ is indicative of successful reduction in overall excitability by grafting WT MGE cells into the Stg V1.

We next reasoned that a successful reduction in excitability decreases slow rhythmic activity that is associated with epileptic activity in vivo (Bazhenov et al. 2008). To test this, we examined the rhythmic structure of network activity in our slice data. Charting of oscillatory structure revealed that control Stg slices exhibited the most pronounced, WTs the lowest, and GStg-V1s intermediate changes in oscillations at low frequencies (Fig. 6*B*). To further evaluate if MGE grafting decreased the coupling of neurons and therefore excitability in V1, we examined correlations between spiking activity on pairs of electrodes during elevated K^+ epoch. The correlation of the timing of APs between pairs of electrodes in controls was significantly greater than both those in WT and GStg-V1 slices (Fig. 6*C*; 0.22 ± 0.002 for WT, black; 0.29 ± 0.006 for control Stgs, red; and 0.24 ± 0.008; $n =$ 1896, 1448, and 1097 electrode pairs, respectively). These data suggest that the synchronized activity, characteristic of epilepsy, is significantly reduced in Stg slices that received WT MGE grafts. Therefore, the 3 distinct measures of network-level activity in response to excitability, firing rate, oscillation structure, and correlations all confirm the reduction in excitability following early postnatal MGE grafting in V1.

Discussion

A current understanding of the etiology of AE is centered on pathological network dynamics in CTC loops through altered synaptic transmission in the reticular thalamic nucleus (van Luijtelaar and Sitnikova 2006; Lacey et al. 2012; Tenney and Glauser 2013). Yet, the causal mechanisms by which the Stargazin mutation alters network excitability have remained elusive (Chetkovich 2009). Stg mice were selected for this study as they exhibit frequent spike-wave discharges that result in spontaneous absence-like seizures caused by a single autosomal gene mutation, which provides a highly suitable model of AE with characteristics similar to the human condition (Letts 2005). The Stg mutation was mapped to a locus encoding for the gamma subunit 2 of the voltage-dependent calcium

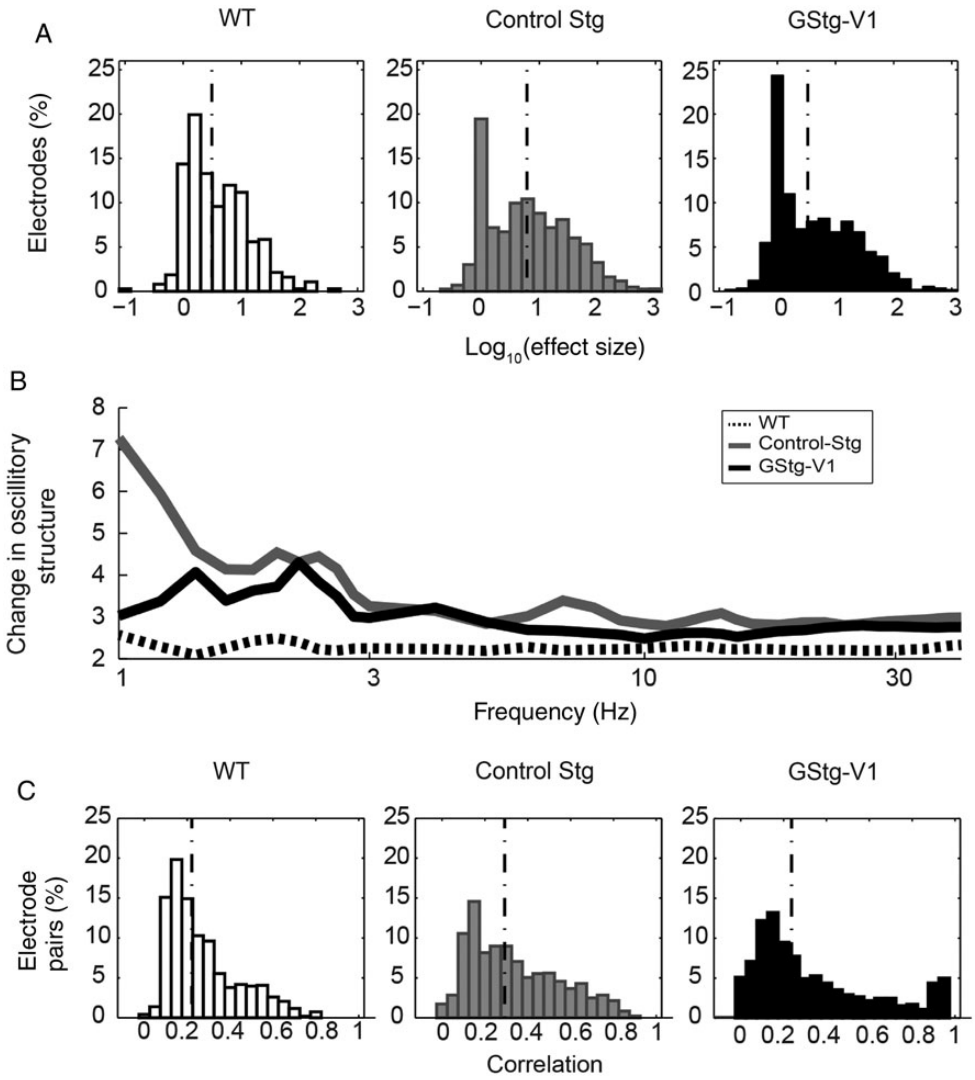

Figure 6. MGE grafting reduces correlated and slow rhythmic responses to an excitability challenge. (*A*) Histograms of the logarithmic effect size of elevated K^+ aCSF on FR for all electrodes, with medians indicated by dashed/dotted lines. Control Stg slices (grey) were significantly more affected by elevated K^+ aCSF than both WT (open bars) and GStg-V1 (black) slices, $P < 0.05$. (*B*) Spectral density for activity in elevated K^+ normalized by activity in control aCSF. Control Stg slices (grey line) had a greater oscillatory structure in low frequencies, while WT slices (dotted line) exhibited less oscillatory structure. Oscillatory structure of GStg-V1 slices (black line) decreased below control Stgs. (*C*) Histograms of correlation in elevated K^+ aCSF, with medians indicated by dashed/dotted lines. Activity in control Stg slices (grey) was significantly more correlated than both in WT (open bars) and GStg-V1 (black), $P < 0.05$.

channel (Cacng2), which results in inappropriate Ca^{2+} entry (Letts et al. 1998) and disrupted AMPA receptor trafficking (Letts 2005) in affected neurons. Loss of Cacng2 function has also been associated with attenuation of its cell adhesive effects (Price et al. 2005) and upregulated expression of synapsins in the cerebral cortex (Meng et al. 2006).

The Stg mutation was recently reported to selectively affect PV expressing GABAergic interneurons in the cortex, resulting in their faulty responsiveness to glutamatergic inputs (Maheshwari et al. 2013). This defect was suggested to be a possible root for unintended and paradoxical effects of antiepileptic drugs on AE seizures. Thus, it is conceivable that Stg defects result in perturbed connectivity and consequent aberrant network activity in the cortex of Stg mice. We were surprised that only a small fraction of grated MGE neurons differentiated into PV+ interneurons at the endpoints set in our study (P14–P21), since a past study suggested that up to 50% of MGE-derived interneurons differentiate into PV+ neurons in the cortex by P14 in mice (Flames et al. 2007). In another report where MGE cells were grafted into P0 mice similar to our study, percentages of PV+ grafted cells were between 20 and 45% in different layers of the cortex (Wang et al. 2010). These differences could be due to our harvesting of MGE grafts a day earlier (E12.5 here vs. E13.5 in both past studies), or the different age of the host brains in the study by Flames et al. (P0 here vs. E13.5). Regardless, in the absence of obvious correlation between the prevalence of PV+ cells in our population of grafted MGE cells and the degree of rescued indices in GStg-V1 mice, we cannot designate the rescue to differentiation of WT PV+ interneurons at this juncture.

Our study represents the first report of utilizing c-Fos mapping for identification of region-specific pathological network activity to target MGE grafting. Our findings indicate that activity reported by c-Fos expression was "locked" in several sensory cortices of Stg brains during prolonged AE seizures. Interestingly, similar "locking' of neuronal activities has

been reported in several somatosensory areas of other AE models (Tenney et al. 2004; David et al. 2008; Mishra et al. 2011; van Raay et al. 2012). To our surprise, targeted grafting of MGE cells into one of these hotspots (V1) was highly successful in treating AE-like phenotypes in Stg mice, which massively eliminated the early postnatal mortality rate of this strain. Our findings are in agreement with previous reports that AE is reversible through inactivation of the cortex (Polack et al. 2009; Gulhan et al. 2010). We noted some cell spreading following grafting of MGE cells into V1 of neonatal mice, which matches previous reports (Alvarez-Dolado et al. 2006). Taken together with the control results whereby MGE grafting in the frontal cortices had no effect Stg seizures, it is reasonable to conclude that WT MGE cells outside V1 are unlikely to have contributed to the profound behavioral reversal of AE episodes in Stg mice. Thus, MGE grafting into the primary visual cortices is a potentially promising approach for treating approximately 30% of AE patients who are estimated to be pharmacoresistant (Ollivier et al. 2009).

Our slice MEA electrophysiology of cortical networks further confirmed alterations in excitability at the cortical level in the absence of thalamic input. Indeed, previously reported enhanced excitability in layer V pyramidal neurons in the temporoparietal region of Stg mice (Di Pasquale et al. 1997) may represent a driving factor for the elevated cortical excitability measured by increase in multiunit firing demonstrated here. Increases in extracellular K^+ concentrations have long been associated with pathological hyperexcitability in the cortex; however, a causal role for K^+ in epileptic seizures remains of debate (Frohlich et al. 2008). Here, we used moderate elevation of K^+ as a tool to probe the response of the V1 network in slices to conditions of increased excitability. This approach was motivated by the assumption that increased responses to such an excitability challenge correspond to an increased propensity to generate epileptiform activity in vivo. Epileptic seizures represent transient epochs of electric activity that are distinctly organized when compared with normal physiological activity. Typically, enhanced temporal synchrony is a key feature of seizure activity. We therefore further investigated the spatiotemporal structure of the spontaneous network activity in acute slices. We found signatures of increased excitability (1) at the level of the temporal structure of spontaneous network activity and (2) at the level of pairwise interactions of different locations with the cortical network measured by correlation. Importantly, these spatiotemporal features of heightened excitability and therefore of propensity to generate electrographic seizures were significantly attenuated by MGE transplantation.

Taken together with the fact that targeting MGE grafts to a single element of the sensory networks at the level of the cortex profoundly reduces displays of AE phenotypes, our findings raise important clinical and mechanistic hypotheses. For example, targeting a single element of the CTC loop (V1) with a presumed modest increase in functional synaptic inhibition (based on the low density of integrated GABAergic neurons in V1 and other regions) can dramatically modulate the overall dynamics of networks underlying AE episodes. Therefore, MGE grafting may function as a unique tool for delineating the molecular, cellular, and physiological mechanisms underlying the role of visual and somatosensory networks in AE seizures. This approach may also enable the development of new therapeutic strategies for neurological disorders characterized by aberrant network dynamics other than AE.

The major obstacle in translating MGE grafting to human patients is obtaining sources of human cells that are comparable to mouse MGE cells. For example, prospective programming of MGE-like cells in induced pluripotent stem cells (Danjo et al. 2011), or human (Liu et al. 2013) and mouse (Au et al. 2013; Petros et al. 2013) embryonic stem cells, could be used as an alternative to harvesting MGE cells from human embryos. Potential reprogramming of endogenous quiescent stem cells in the adult subventricular zone may also provide an attractive pool of GABAergic cells for cell-based therapies (Ohira et al. 2010). Notwithstanding the limitations and challenges in cell-based therapies in the human central nervous system, our findings provide a potential treatment strategy for AE by grafting GABAergic interneurons into V1, a brain region that is highly accessible with minimally invasive surgeries.

Funding

This work was supported in part by an NIH grant (R01NS062182) to H.T.G., and by institutional funds to H.T.G. (NCSU) and F.F. (UNC Chapel Hill).

Notes

Conflict of Interest: None declared.

References

Alvarez-Dolado M, Calcagnotto ME, Karkar KM, Southwell DG, Jones-Davis DM, Estrada RC, Rubenstein JL, Alvarez-Buylla A, Baraban SC. 2006. Cortical inhibition modified by embryonic neural precursors grafted into the postnatal brain. J Neurosci. 26:7380–7389.

Anderson SA, Eisenstat DD, Shi L, Rubenstein JL. 1997. Interneuron migration from basal forebrain to neocortex: dependence on Dlx genes. Science. 278:474–476.

Au E, Ahmed T, Karayannis T, Biswas S, Gan L, Fishell G. 2013. A modular gain-of-function approach to generate cortical interneuron subtypes from ES cells. Neuron. 80:1145–1158.

Baraban SC, Southwell DG, Estrada RC, Jones DL, Sebe JY, Alfaro-Cervello C, Garcia-Verdugo JM, Rubenstein JL, Alvarez-Buylla A. 2009. Reduction of seizures by transplantation of cortical GABAergic interneuron precursors into Kv1.1 mutant mice. Proc Natl Acad Sci USA 106:15472–15477.

Bazhenov M, Timofeev I, Frohlich F, Sejnowski TJ. 2008. Cellular and network mechanisms of electrographic seizures. Drug Discov Today Dis Models 5:45–57.

Beydoun A, D'Souza J. 2012. Treatment of idiopathic generalized epilepsy—a review of the evidence. Expert Opin Pharmacother. 13:1283–1298.

Blumenfeld H. 2005. Cellular and network mechanisms of spike-wave seizures. Epilepsia. 46(Suppl 9):21–33.

Calcagnotto ME, Ruiz LP, Blanco MM, Santos-Junior JG, Valente MF, Patti C, Frussa-Filho R, Santiago MF, Zipancic I, Alvarez-Dolado M et al. 2010. Effect of neuronal precursor cells derived from medial ganglionic eminence in an acute epileptic seizure model. Epilepsia. 51(Suppl 3):71–75.

Chetkovich D. 2009. Thalamic reticular neurons are unexcited by new stargazer seizure mechanism. Epilepsy Curr. 9:59–61.

Crunelli V, Leresche N, Cope DW. 2012. GABA-A receptor function in typical absence seizures. In: Noebels JL, Avoli M, Rogawski M, Olsen R, Delgado-Escueta A, editors. Jasper's basic mechanisms of the epilepsies. MD (USA): National Center for Biotechnology Information.

Danjo T, Eiraku M, Muguruma K, Watanabe K, Kawada M, Yanagawa Y, Rubenstein JL, Sasai Y. 2011. Subregional specification of embryonic stem cell-derived ventral telencephalic tissues by timed and combinatory treatment with extrinsic signals. J Neurosci. 31:1919–1933.

David O, Guillemain I, Saillet S, Reyt S, Deransart C, Segebarth C, Depaulis A. 2008. Identifying neural drivers with functional MRI: an electrophysiological validation. PLoS Biol. 6:2683–2697.

de Boer HM, Mula M, Sander JW. 2008. The global burden and stigma of epilepsy. Epilepsy Behav. 12:540–546.
Di Pasquale E, Keegan KD, Noebels JL. 1997. Increased excitability and inward rectification in layer V cortical pyramidal neurons in the epileptic mutant mouse Stargazer. J Neurophysiol. 77:621–631.
Flames N, Pla R, Gelman DM, Rubenstein JL, Puelles L, Marin O. 2007. Delineation of multiple subpallial progenitor domains by the combinatorial expression of transcriptional codes 1. J Neurosci. 27:9682–9695.
Frohlich F, Bazhenov M, Iragui-Madoz V, Sejnowski TJ. 2008. Potassium dynamics in the epileptic cortex: new insights on an old topic. Neuroscientist. 14:422–433.
Ghashghaei HT, Barbas H. 2001. Neural interaction between the basal forebrain and functionally distinct prefrontal cortices in the rhesus monkey. Neuroscience. 103:593–614.
Ghashghaei HT, Barbas H. 2002. Pathways for emotion: interactions of prefrontal and anterior temporal pathways in the amygdala of the rhesus monkey. Neuroscience. 115:1261–1279.
Ghashghaei HT, Hilgetag CC, Barbas H. 2007. Sequence of information processing for emotions based on the anatomic dialogue between prefrontal cortex and amygdala. Neuroimage. 34:905–923.
Gulhan AR, Tezcan K, Carcak N, Sakalli E, Akin D, Onat FY. 2010. Localized cortical injections of ethosuximide suppress spike-and-wave activity and reduce the resistance to kindling in genetic absence epilepsy rats (GAERS). Epilepsy Res. 89:7–16.
Hunt RF, Girskis KM, Rubenstein JL, Alvarez-Buylla A, Baraban SC. 2013. GABA progenitors grafted into the adult epileptic brain control seizures and abnormal behavior. Nat Neurosci. 16:692–697.
Jacquet BV, Ruckart P, Ghashghaei HT. 2010. An organotypic slice assay for high-resolution time-lapse imaging of neuronal migration in the postnatal brain. J Vis Exp. 46:2486.
Killory BD, Bai X, Negishi M, Vega C, Spann MN, Vestal M, Guo J, Berman R, Danielson N, Trejo J et al. 2011. Impaired attention and network connectivity in childhood absence epilepsy. Neuroimage. 56:2209–2217.
Lacey CJ, Bryant A, Brill J, Huguenard JR. 2012. Enhanced NMDA receptor-dependent thalamic excitation and network oscillations in stargazer mice. J Neurosci. 32:11067–11081.
Letts VA. 2005. Stargazer—a mouse to seize! Epilepsy Curr. 5:161–165.
Letts VA, Felix R, Biddlecome GH, Arikkath J, Mahaffey CL, Valenzuela A, Bartlett FS, Mori Y, Campbell KP, Frankel WN. 1998. The mouse stargazer gene encodes a neuronal Ca^{2+}-channel gamma subunit. Nat Genet. 19:340–347.
Liu Y, Weick JP, Liu H, Krencik R, Zhang X, Ma L, Zhou GM, Ayala M, Zhang SC. 2013. Medial ganglionic eminence-like cells derived from human embryonic stem cells correct learning and memory deficits. Nat Biotechnol. 31:440–447.
Maheshwari A, Nahm WK, Noebels JL. 2013. Paradoxical proepileptic response to NMDA receptor blockade linked to cortical interneuron defect in stargazer mice. Front Cell Neurosci. 7:156.
Meeren H, van LG, Lopes da SF, Coenen A. 2005. Evolving concepts on the pathophysiology of absence seizures: the cortical focus theory. Arch Neurol. 62:371–376.
Meng H, Walker N, Su Y, Qiao X. 2006. Stargazin mutation impairs cerebellar synaptogenesis, synaptic maturation and synaptic protein distribution. Brain Res. 1124:197–207.
Mishra AM, Ellens DJ, Schridde U, Motelow JE, Purcaro MJ, Desalvo MN, Enev M, Sanganahalli BG, Hyder F, Blumenfeld H. 2011. Where fMRI and electrophysiology agree to disagree: corticothalamic and striatal activity patterns in the WAG/Rij rat. J Neurosci. 31:15053–15064.
Ohira K, Furuta T, Hioki H, Nakamura KC, Kuramoto E, Tanaka Y, Funatsu N, Shimizu K, Oishi T, Hayashi M et al. 2010. Ischemia-induced neurogenesis of neocortical layer 1 progenitor cells. Nat Neurosci. 13:173–179.
Ollivier ML, Dubois MF, Krajinovic M, Cossette P, Carmant L. 2009. Risk factors for valproic acid resistance in childhood absence epilepsy. Seizure. 18:690–694.
Paxinos G, Franklin KBJ. 2001. The mouse brain in stereotaxic coordinates. San Diego (CA): Academic Press.
Paxinos G, Halliday G, Watson C, Koutcherov Y, Wang HQ. 2007. Atlas of the developing mouse brain. San Diego (CA): Elsevier.
Petros TJ, Maurer CW, Anderson SA. 2013. Enhanced derivation of mouse ESC-derived cortical interneurons by expression of Nkx2.1. Stem Cell Res. 11:647–656.
Polack PO, Mahon S, Chavez M, Charpier S. 2009. Inactivation of the somatosensory cortex prevents paroxysmal oscillations in cortical and related thalamic neurons in a genetic model of absence epilepsy. Cereb Cortex. 19:2078–2091.
Price MG, Davis CF, Deng F, Burgess DL. 2005. The alpha-amino-3-hydroxyl-5-methyl-4-isoxazolepropionate receptor trafficking regulator "Stargazin" is related to the claudin family of proteins by its ability to mediate cell-cell adhesion. J Biol Chem. 280:19711–19720.
Schmidt SL, Chew EY, Bennett DV, Hammad MA, Frohlich F. 2013. Differential effects of cholinergic and noradrenergic neuromodulation on spontaneous cortical network dynamics. Neuropharmacology. 72:259–273.
Seneviratne U, Cook M, D'Souza W. 2012. The prognosis of idiopathic generalized epilepsy. Epilepsia. 53:2079–2090.
Sherman SM, Guillery RW. 2011. Distinct functions for direct and transthalamic corticocortical connections. J Neurophysiol. 106:1068–1077.
Southwell DG, Froemke RC, Alvarez-Buylla A, Stryker MP, Gandhi SP. 2010. Cortical plasticity induced by inhibitory neuron transplantation. Science. 327:1145–1148.
Tenney JR, Duong TQ, King JA, Ferris CF. 2004. fMRI of brain activation in a genetic rat model of absence seizures. Epilepsia. 45:576–582.
Tenney JR, Glauser TA. 2013. The current state of absence epilepsy: can we have your attention? Epilepsy Curr. 13:135–140.
Thompson K. 2009. Transplantation of GABA-producing cells for seizure control in models of temporal lobe epilepsy. Neurotherapeutics. 6:284–294.
van Luijtelaar G, Sitnikova E. 2006. Global and focal aspects of absence epilepsy: the contribution of genetic models. Neurosci Biobehav Rev. 30:983–1003.
van Raay L, Jovanovska V, Morris MJ, O'Brien TJ. 2012. Focal administration of neuropeptide Y into the S2 somatosensory cortex maximally suppresses absence seizures in a genetic rat model. Epilepsia. 53:477–484.
Waldau B. 2010. Stem cell transplantation for enhancement of learning and memory in adult neurocognitive disorders. Aging Dis. 1:60–71.
Wang Y, Dye CA, Sohal V, Long JE, Estrada RC, Roztocil T, Lufkin T, Deisseroth K, Baraban SC, Rubenstein JL. 2010. Dlx5 and Dlx6 regulate the development of parvalbumin-expressing cortical interneurons. J Neurosci. 30:5334–5345.
West MJ, Gundersen HJ. 1990. Unbiased stereological estimation of the number of neurons in the human hippocampus. J Comp Neurol. 296:1–22.